Comput. Methods Appl. Mech. Engrg. 199 (2010) 2655–2662

Contents lists available at ScienceDirect

Comput. Methods Appl. Mech. Engrg.

journal homepage: www.elsevier.com/locate/cma

A fourth order finite difference method for waveguides with curved perfectly conducting boundaries

Shan Zhao *

Department of Mathematics, University of Alabama, Tuscaloosa, AL 35487, USA

ARTICLE INFO

Article history:
Received 9 November 2009
Received in revised form 13 May 2010
Accepted 15 May 2010
Available online 4 June 2010

Keywords:
High order finite difference method
Matched interface and boundary method
Perfectly electric conducting boundary
Staircasing error
Waveguide theory

ABSTRACT

A novel high order finite difference method is introduced for optical waveguides with smoothly curved perfectly electric conducting (PEC) boundaries. The proposed method shares some similarities with our previous matched interface and boundary (MIB) methods developed for treating dielectric interfaces of optical waveguides, such as the use of a simple Cartesian grid, the standard finite difference schemes, and fictitious values. However, the PEC boundary conditions have a physical nature quite different from that of the jump conditions at the dielectric interfaces, i.e., all six electric and magnetic field components are prescribed in the jump conditions, while only three of them are known at the PEC walls. Consequently, the previously developed MIB methods are not applicable to deal with the perfectly conducting boundaries. To overcome this difficulty, a novel ray-casting fictitious domain method is constructed to enforce the PEC conditions along the normal direction. Such a boundary implementation couples the transverse magnetic field components so that the resulting ray-casting MIB method is a full vectorial approach for the modal analysis of optical waveguides. The new MIB method is validated by considering both homogeneous and inhomogeneous waveguides. Numerical results confirm the designed fourth order of accuracy.

© 2010 Elsevier B.V. All rights reserved.

1. Introduction

It is well known that the conventional Cartesian grid based numerical methods will be degraded to only first order accuracy when modeling curved perfectly electric conducting (PEC) walls, due to the so-called staircasing error. To circumvent the staircasing error, one possible way is fitting the mesh to the boundaries, via the use of body-conforming grids or unstructured grids. For example, a nonuniform triangular mesh based full vectorial finite difference formulation has been proposed for solving optical waveguides in [1]. In [2], a curvilinear mapping technique has been introduced to the multidomain pseudospectral method for waveguide analysis. Using unstructured grids, the finite element method is very flexible in handling geometrically complex problems. Recently, some further improvements to the finite element analysis of optical waveguides have been accomplished by using various curvilinear/isoparametric elements [3–6] to achieve a better fit at the curved boundaries or interfaces.

What are more relevant to the present study are the Cartesian grid methods for treating curved material boundaries and interfaces. In such methods, Cartesian grids are employed so that the simplicity of the conventional finite difference methods is maintained, while some special treatments are required only adjacent to physical boundaries. In the time domain, various promising finite difference time domain (FDTD) methods have been proposed to overcome the staircasing error at the PEC boundaries, including conformal FDTD methods [7–10], flux limiting embedded boundary method [11], consistent boundary conditions [12], and so on. In these methods, the staircasing error is eliminated by locally modifying the finite difference weights so that not only the PEC boundary conditions can be satisfied, but also the original FDTD stability constrains can be maintained.

In the frequency domain, several Cartesian grid methods have been developed for solving a related problem – the dielectric interface problem. In an interface problem, the field solution loses its regularity across the irregular material interfaces, so that special local treatments in which the interface jump conditions are properly imposed in the discretization, are essential to achieve high order of accuracy [13]. For simple interfaces which are straight and align with one coordinate direction, up to 12th order finite difference waveguide solvers have been reported in the literature [14–16]. For optical waveguide with curved interfaces, a second order Cartesian grid method was first presented by Chiang et al. [17]. Recently, we have proposed novel full vectorial matched interface and boundary (MIB) methods [18,19], which achieve a fourth order convergence irrespective of the presence of curved interfaces.

However, the previously developed MIB interface schemes [18,19] cannot be reformulated to solve the present PEC boundary problem. The essential difficulty is due to a different nature of

* Tel.: +1 205 3485155; fax: +1 205 3487067.
E-mail address: szhao@bama.ua.edu

0045-7825/$ - see front matter © 2010 Elsevier B.V. All rights reserved.
doi:10.1016/j.cma.2010.05.005

the physical conditions underlying the dielectric interfaces and PEC walls. At the dielectric interface, jump conditions are available which analytically relate field solutions across the interface, while at the PEC wall, some specific values of field solutions are known. Nevertheless, there are six jump conditions prescribed so that all six electric and magnetic field components are taken care of at the dielectric interfaces, while only three electric and magnetic field components are specified at the PEC walls. This calls for novel formulations in generalizing the MIB method to solve irregular PEC boundaries. On the other hand, we note that for regular PEC boundaries of a rectangular domain, the PEC boundary conditions reduce to the standard Dirichlet and Neumann conditions along a Cartesian direction. For such a simple problem, a boundary closure procedure for arbitrarily high order finite difference methods is available in [20,21].

The objective of this paper is to introduce a novel ray-casting MIB method for dealing with smoothly curved PEC boundaries. The unique feature of the ray-casting MIB method is to impose the PEC conditions only along the normal direction. The new MIB scheme and the previous MIB interface method [18] are all based on an effective use of fictitious values, an idea which was first proposed in a scalar MIB method for solving Maxwell's equations with straight interfaces [13], and was subsequently generalized to treat curved interfaces for solving the Poisson equation [22]. Nevertheless, the fictitious values are independent from each other in the present scheme, while the fictitious values in the previous MIB methods [13,22,18,19] are determined in pairs.

The rest of this paper is organized as follows: Section 2 is devoted to theory and algorithm of the proposed ray-casting MIB method. In Section 3, both homogeneous and inhomogeneous waveguides with curved PEC boundaries will be employed to validate the proposed approach. Finally, a conclusion ends this paper.

2. Formulation and discretization

In this section, we first present the governing equations and boundary conditions for the eigenmode analysis of optical waveguides. The general procedure of the matched interface and boundary (MIB) method will be described next. A new ray-casting MIB method will then be proposed and the discretization details are given.

2.1. Physical equations and boundary conditions

Consider a linear isotropic optical waveguide with a smooth perfectly electric conducting (PEC) boundary Γ. The optical waveguides are normally homogeneous in the z-direction so that one can assume the field solution varies as $e^{-j\beta z}$ along the z-direction, where β is the propagation constant and $j=\sqrt{-1}$. A large enough rectangular computational domain is assumed to enclose the PEC boundary as an embedded boundary. For simplicity, we will consider only magnetic field intensity $\mathbf{H}$. Equations for the electric field intensity $\mathbf{E}$ can be similarly treated. By using the source-free Maxwell's equations, the following vector wave equation can be derived for $\mathbf{H}$

$$\nabla\times\left(\frac{1}{\epsilon}\nabla\times\mathbf{H}\right)-k_0^2\mu\mathbf{H}=0, \tag{1}$$

where ϵ and μ are, respectively, the relative permittivity and permeability coefficients, and $k_0=2\pi/\lambda$ is the free space wavenumber with λ being the free space wavelength. By using vector analysis and the z-direction dependence in terms of β, Eq. (1) reduces to [19]

$$\nabla_t^2\mathbf{H}+k_0^2\epsilon\mu\mathbf{H}=\beta^2\mathbf{H}-\epsilon\left(\nabla_t\frac{1}{\epsilon}\cdot\nabla_t\right)\mathbf{H}, \tag{2}$$

where ∇_t is the transverse part of ∇.

For the commonly used step-index optical waveguides, the dielectric coefficient ϵ is a piecewise constant. Consequently, except on the interface separating two dielectric media, the magnetic field $\mathbf{H}$ satisfies the vector Helmholtz equation

$$\nabla_t^2\mathbf{H}+k_0^2\epsilon\mu\mathbf{H}=\beta^2\mathbf{H}, \tag{3}$$

within each homogeneous medium. Because a Cartesian grid method makes use of a simple uniform grid throughout the domain, the governing equations are better prescribed in terms of Cartesian components of $\mathbf{H}$, i.e., H^x, H^y, and H^z. In particular, these Cartesian components individually satisfy the scalar Helmholtz equation within each homogeneous medium

$$\frac{\partial^2 H}{\partial x^2}+\frac{\partial^2 H}{\partial y^2}+k_0^2\epsilon\mu H=\beta^2 H, \tag{4}$$

where H stands for H^x, H^y, or H^z.

To recover the effect of the singular term being dropped in (2), some necessary conditions at material interface have to be imposed in the numerical discretization [18,19]. Such conditions are known as the jump conditions in the literature and they relate field solutions analytically in both media

$$\begin{aligned}&\hat{\mathbf{n}}\times(\mathbf{E}^+-\mathbf{E}^-)=0,\quad \hat{\mathbf{n}}\cdot(\epsilon^+\mathbf{E}^+-\epsilon^-\mathbf{E}^-)=0,\\ &\hat{\mathbf{n}}\times(\mathbf{H}^+-\mathbf{H}^-)=0,\quad \hat{\mathbf{n}}\cdot(\mu^+\mathbf{H}^+-\mu^-\mathbf{H}^-)=0,\end{aligned} \tag{5}$$

where the superscript, $-$ or $+$, denotes the limiting value of a function from one side or the other of the interface. Here $\hat{\mathbf{n}}$ is the unit vector normal to the interface. It is noted that the scalar Helmholtz equation (4) is valid for step-index inhomogeneous waveguide, provided that the jump conditions (5) are enforced at the interface too.

The previously developed matched interface and boundary (MIB) methods for optical waveguides are numerical approaches to impose jump conditions (5) at dielectric interfaces of arbitrary shape [18,19]. However, such MIB methods can not be directly generalized to solve the present PEC boundary problem, because the PEC boundary conditions have a different nature. To illustrate the idea, consider a point P to be either a point on the material interface or a point on the PEC boundary. Assume the curvature at point P to be κ or the effective radius be $R=1/\kappa$. Geometrically, this defines a osculating circle and a corresponding local cylindrical coordinate system $(\vec{\rho},\vec{\varphi},\vec{z})$ [19]. On such a local grid system, the jump conditions (5) reduce to the following six jump conditions for the cylindrical components of $\mathbf{E}$ and $\mathbf{H}$

$$[H^z]=0,\quad [H^\varphi]=0,\quad [\mu H^\rho]=0,\quad [E^z]=0,\quad [E^\varphi]=0,\quad [\epsilon E^\rho]=0, \tag{6}$$

where $[u]$ denotes a function jump for a scalar function u, i.e., $[u]:=\lim_{\rho\to R^+}u-\lim_{\rho\to R^-}u$.

On the other hand, at a PEC boundary point P, we have the following boundary conditions

$$\hat{\mathbf{n}}\times\mathbf{E}=0,\quad \hat{\mathbf{n}}\cdot(\epsilon\mathbf{E})=q_s,\quad \hat{\mathbf{n}}\times\mathbf{H}=\mathbf{J}_s,\quad \hat{\mathbf{n}}\cdot(\mu\mathbf{H})=0, \tag{7}$$

where q_s and $\mathbf{J}_s$ is, respectively, the induced surface electric charge density and electric current density. These densities are generally nonzero since there are plenty of free charges that are confined to a very thin layer on the surface of the perfect conductor. Nevertheless, such nonzero values are usually unknown in the typical electromagnetic applications, such as the present eigenvalue analysis of optical waveguides. Therefore, in the filed of computational electromagnetics (CEM), two unfixed boundary conditions have to be neglected in (7). This gives rise to the commonly used PEC boundary conditions in the literature

$$\hat{\mathbf{n}}\times\mathbf{E}=0,\quad \hat{\mathbf{n}}\cdot(\mu\mathbf{H})=0. \tag{8}$$

In the local cylindrical coordinate, Eq. (8) represents three PEC conditions

$$E^{\varphi} = 0, \quad E^{z} = 0, \quad \mu H^{\rho} = 0. \tag{9}$$

In comparing the interface jump conditions (6) with the PEC boundary conditions (9), one might argue that the PEC conditions are mathematically stronger in the sense that they specify the zero values of fields at the PEC walls, while the jump conditions only provide a connection across the dielectric interfaces. However, we actually have six jump conditions for each field component in (6), whereas one does not know the function behavior for the other three field components that are missing in (9). This is essentially why the interface methods cannot be directly generalized to solve the PEC boundary problems.

2.2. Full vectorial finite difference methods based on the MIB

We will describe the general procedure of the MIB method in this subsection. We first assume $\mu = 1$ as in most common electromagnetic applications. A uniform mesh is employed throughout the domain. A typical PEC boundary segment and the surrounding Cartesian nodes are shown in Fig. 1. Because we will solve step-index optical waveguides by using the previously developed MIB methods [18,19] to treat the dielectric interfaces in our numerical tests, we will formulate the proposed MIB method for the PEC walls in the same setting. In particular, a full vectorial formulation in terms of transverse magnetic field components (H^x,H^y) will be considered.

Both H^x and H^y satisfy the scalar Helmholtz equation (4). The standard fourth order finite difference scheme will be employed to approximate both x and y derivatives of (4) in the MIB method. For example, denoting $H_{i,j} = H(x_i, y_j)$, one has

$$\frac{\partial^2}{\partial x^2} H_{i,j} \approx \frac{1}{\Delta x^2}\left(-\frac{1}{12}H_{i-2,j} + \frac{4}{3}H_{i-1,j} - \frac{5}{2}H_{i,j} + \frac{4}{3}H_{i+1,j} - \frac{1}{12}H_{i+2,j}\right). \tag{10}$$

Such an approximation will be used whenever (x_i, y_j) is within the PEC boundary. For (x_i, y_j) near the PEC boundary Γ, the approximation (10) involves grid nodes outside the dielectric medium. A universal rule of the MIB is that to approximate function or its derivative on one side of interface/boundary, one never *directly* refers to function values from the other side. Instead, fictitious values from the other side of the interface/boundary will be supplied. For example, for the particular grid topology shown in Fig. 1, we have the following modified finite difference approximation for the y derivative

$$\frac{\partial^2}{\partial y^2} H_{i,j} \approx \frac{1}{\Delta y^2}\left(-\frac{1}{12}H_{i,j-2} + \frac{4}{3}H_{i,j-1} - \frac{5}{2}H_{i,j} + \frac{4}{3}\widetilde{H}_{i,j+1} - \frac{1}{12}\widetilde{H}_{i,j+2}\right), \tag{11}$$

where $\widetilde{H}_{i,j+1}$ denotes the fictitious value at the node (x_i, y_{j+1}). Such an approximation maintains the fourth order of accuracy, provided that $\widetilde{H}_{i,j+1}$ and $\widetilde{H}_{i,j+2}$ are accurately estimated.

To discretize the Helmholtz equation (4) on all interior nodes by using the fourth order finite difference, it is sufficient to accurately generate two layers of fictitious nodes coating the PEC wall Γ. Note that on each fictitious node, two fictitious values $\widetilde{H}^x$ and $\widetilde{H}^y$ are needed. To compute them, we actually solve fictitious values $\widetilde{H}^{\rho}$ and $\widetilde{H}^{\varphi}$ on the same node first, because the PEC conditions will be prescribed in terms of local magnetic components. Then, the following coordinate transformations shall be performed to relate global field components H^x and H^y and local field components H^{ρ} and H^{φ} at regular node or fictitious node

$$H^{\rho} = \cos\varphi H^x + \sin\varphi H^y, \quad H^{\varphi} = -\sin\varphi H^x + \cos\varphi H^y, \tag{12}$$

$$H^x = \cos\varphi H^{\rho} - \sin\varphi H^{\varphi}, \quad H^y = \sin\varphi H^{\rho} + \cos\varphi H^{\varphi}. \tag{13}$$

With these transformations, the Helmholtz equation (4) can be solved throughout in terms of (H^x,H^y). On the other hand, we note that H^{ρ} and H^{φ} do not satisfy the Cartesian Helmholtz equation (4).

The essential part of the MIB method is the fictitious value determination. For elliptic interface problem [22] and electromagnetic interface problem [18,19], a key idea of the MIB fictitious domain treatment is to decompose the higher dimensional interface conditions so that they can be imposed in a one dimensional manner. Normally, besides the zeroth order conditions on function values of field components, the normal and tangential derivative conditions are also required in the MIB algorithm development. To this end, let us investigate the available PEC conditions for the local cylindrical components (H^{ρ},H^{φ}). Based on equation (9), we have $H^{\rho} = 0$ since $\mu = 1$. Differentiating along the boundary, one has $\frac{\partial H^{\rho}}{\partial \varphi} = 0$. However, in general, we do not know the value of normal derivative $\frac{\partial H^{\rho}}{\partial \rho}$. Similarly, for H^{φ}, nothing is available about its value and tangential derivative. Instead, a PEC condition on its normal derivative can be derived. In particular, we consider one Maxwell's equation in the local cylindrical coordinate

$$\frac{\partial E^z}{\partial t} = \frac{1}{\epsilon}\left(\frac{\partial H^{\varphi}}{\partial \rho} + \frac{1}{\rho}H^{\varphi} - \frac{1}{\rho}\frac{\partial H^{\rho}}{\partial \varphi}\right). \tag{14}$$

At the PEC boundary point P, we have $\rho = R$ and $E^z = 0$ at all time so that $\partial E^z/\partial t = 0$. Also, since $\frac{\partial H^{\rho}}{\partial \varphi} = 0$, Eq. (14) reduces to a Robin boundary condition for H^{φ} at P

$$\frac{\partial H^{\varphi}}{\partial \rho} + \frac{1}{R}H^{\varphi} = 0. \tag{15}$$

In summary, we have the following three PEC boundary conditions for local magnetic field components H^{ρ} and H^{φ}

$$H^{\rho} = 0, \quad \frac{\partial H^{\rho}}{\partial \varphi} = 0, \quad \frac{\partial H^{\varphi}}{\partial \rho} + \frac{1}{R}H^{\varphi} = 0. \tag{16}$$

For a comparison, we would like to point out that there are actually six jump conditions for H^{ρ} and H^{φ} at the dielectric interface [18,19]

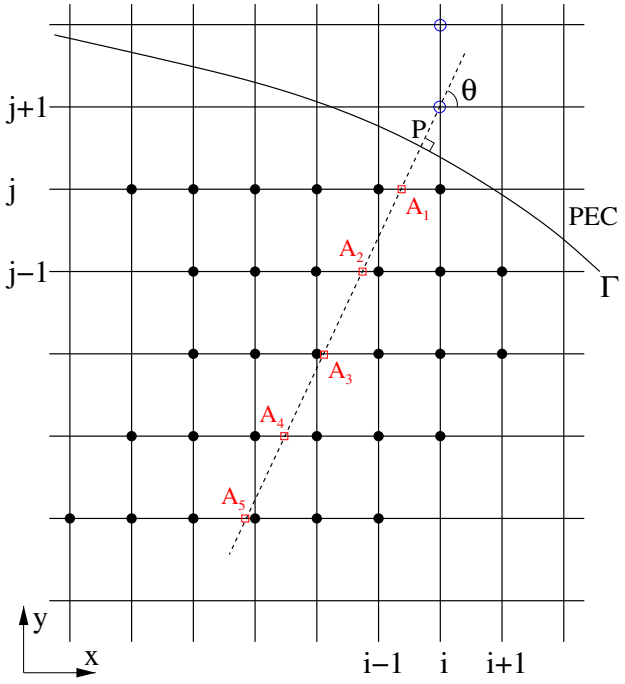

Fig. 1. Illustration of the MIB grid partition. Filled circles: Cartesian nodes; open circles: fictitious nodes; squares: auxiliary nodes.

$$[H^\rho]=0,\quad [H^\varphi]=0,\quad \left[\frac{\partial H^\rho}{\partial \rho}\right]=0,\quad \left[\frac{\partial H^\rho}{\partial \varphi}\right]=0,$$
$$\left[\frac{\partial H^\varphi}{\partial \varphi}\right]=0,\quad \left[\frac{1}{\epsilon}\frac{\partial H^\varphi}{\partial \rho}\right]+\frac{1}{R}\left[\frac{1}{\epsilon}H^\varphi\right]=\frac{1}{R}\left[\frac{1}{\epsilon}\frac{\partial H^\rho}{\partial \varphi}\right]. \tag{17}$$

In other words, both field components (H^ρ, H^φ) and all their normal and tangential derivatives are known at the material interfaces. Nevertheless, this is not the case at the PEC walls. Therefore, alternative fictitious domain treatment has to be constructed at the PEC walls.

2.3. Ray-casting MIB method

To overcome the difficulty associated with the PEC boundary, we propose a novel ray-casting MIB scheme. Unlike the previous MIB methods [18,19] which decompose the jump conditions into Cartesian directions x or y, the ray-casting MIB scheme will discretize the PEC conditions (16) only along the normal direction. Thus, the second equation in (16), i.e., the tangential derivative condition, is not needed in the present approach.

To illustrate the idea, let us consider the determination of $\widetilde{H}^\rho$ and $\widetilde{H}^\varphi$ on the fictitious node (x_i, y_{j+1}) in Fig. 1. An auxiliary normal line will be generated, which is both passing the node (x_i, y_{j+1}) and perpendicular to the Γ at an intersection point P. In order to maintain the fourth order of accuracy, five auxiliary nodes inside the PEC wall shall be employed to discretize (16). Denote the angle between the auxiliary normal line and the positive x direction to be θ. One needs to consider two scenarios depending on whether the auxiliary line meets the x or y grid line first inside the PEC wall. Computationally, this can be determined by examining the relation between θ and the mesh angle $\tan^{-1}(\Delta y/\Delta x)$. For example, when $\Delta y = \Delta x$, if $\frac{3\pi}{4} \geqslant \theta \geqslant \frac{\pi}{4}$ or $\frac{7\pi}{4} \geqslant \theta \geqslant \frac{5\pi}{4}$, these five auxiliary nodes will be chosen as the intersection points of the auxiliary line with five x grid lines. Otherwise, they will be set as the intersection points with five y grid lines. Fig. 1 shows the situation for the former case, while the latter case can be similarly formulated and will not be discussed for simplicity.

As shown in Fig. 1, the five auxiliary nodes are denoted as (x_{A_1}, y_j), (x_{A_2}, y_{j-1}), (x_{A_3}, y_{j-2}), (x_{A_4}, y_{j-3}), and (x_{A_5}, y_{j-4}). Together with the fictitious node (x_i, y_{j+1}), this defines a six-points stencil. The ρ values along this stencil are denoted to be ρ_0 for (x_i, y_{j+1}) and $(\rho_1, \rho_2, \rho_3, \rho_4, \rho_5)$ for the rest five auxiliary nodes. A finite difference approximation kernel differentiating at $\rho = R$ can then be generated based on six ρ values. Consequently, (16) can be discretized along the auxiliary line or the normal direction

$$w_0^0 \widetilde{H}^\rho_{i,j+1} + \sum_{k=1}^{5} w_k^0 H^\rho_{A_k j+1-k} = 0,$$
$$\left(w_0^1 + \frac{w_0^0}{\rho_0}\right)\widetilde{H}^\varphi_{i,j+1} + \sum_{k=1}^{5}\left(w_k^1 + \frac{w_k^0}{\rho_k}\right) H^\varphi_{A_k j+1-k} = 0, \tag{18}$$

where w_k^m for $m = 0, 1$ and $k = 0, 1, \ldots, 5$ are finite difference weights. Here the superscript m represents interpolation ($m = 0$) or the first order derivative approximation ($m = 1$), and the subscript k is for the index of ρ.

By solving two algebraic equations in (18), one attains fictitious values $\widetilde{H}^\rho_{i,j+1}$ and $\widetilde{H}^\varphi_{i,j+1}$ as linear combinations of function values of H^ρ and H^φ on five auxiliary nodes

$$\widetilde{H}^\rho_{i,j+1} = -\frac{1}{w_0^0}\sum_{k=1}^{5} w_k^0 H^\rho_{A_k j+1-k},$$
$$\widetilde{H}^\varphi_{i,j+1} = -\frac{1}{(w_0^1 + \frac{w_0^0}{\rho_0})}\sum_{k=1}^{5}\left(w_k^1 + \frac{w_k^0}{\rho_k}\right) H^\varphi_{A_k j+1-k}. \tag{19}$$

via the coordinate transformation (12) and (13), the fictitious values $\widetilde{H}^x_{i,j+1}$ and $\widetilde{H}^y_{i,j+1}$ will also be some linear combinations of function values of H^x and H^y on five auxiliary nodes. Finally, to attain a full Cartesian grid approach, each auxiliary point will be interpolated along x line by using six nearest nodes exclusively inside the PEC wall, see Fig. 1. We note that there are situations in which no enough nodes are available for the interpolation of the first auxiliary node (x_{A_1}, y_j). In such a case, the first x grid line shall be skipped and the five auxiliary nodes shall be chosen as the intersection points of the normal line with the next five x grid lines. In other words, a down shifting of all involved nodes will be carried out. Such an adaptive procedure works quite well in our experiments.

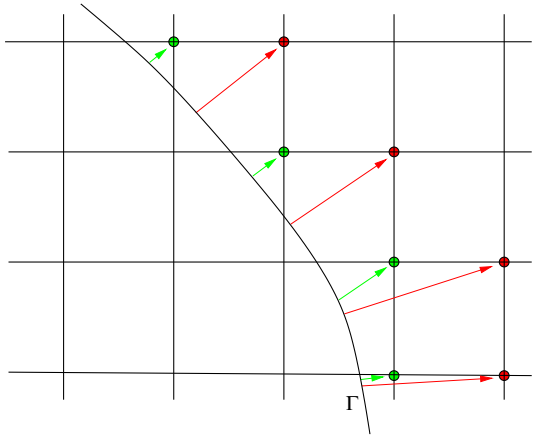

Fig. 2. Illustration of the ray-casting process of the MIB scheme.

In the final ray-casting MIB discretization, each fictitious value of $\widetilde{H}^x$ or $\widetilde{H}^y$ at node (x_i, y_{j+1}) will depend on totally 60 function values of H^x and H^y on 30 Cartesian nodes shown in Fig. 1. To complete the fourth order finite approximation (10), two more fictitious values at node (x_i, y_{j+2}) are required. In the present study, the aforementioned procedure for (x_i, y_{j+1}) can be simply carried out again to resolve $\widetilde{H}^x_{i,j+2}$ and $\widetilde{H}^y_{i,j+2}$ in terms of another set of 60 function values of H^x and H^y. Thus, two fictitious nodes (x_i, y_{j+1}) and (x_i, y_{j+2}) are independent from each other, while in the previous MIB interface schemes [22,18], they are usually coupled. By applying the ray-casting MIB treatment for every possible fictitious point, finally two layers of fictitious points are generated to coat the PEC wall Γ, see Fig. 2. In some sense, these fictitious nodes are constructed as the normal projections of certain PEC boundary points through a ray-casting process.

3. Numerical results

Three waveguide structures involving both homogeneous and inhomogeneous media are employed to validate the proposed ray-casting MIB approach. For all waveguide analyses, only a few dominate modes are considered and the corresponding effective propagation constant $\beta_e = \beta/k_0$ will be calculated and compared with analytical results [23]. In all cases, a large enough square computational domain $[-a, a] \times [-a, a]$ is used. Here the domain size a is usually chosen as a non-integer number such that the boundary intersection and orientation with respect to the Cartesian grid could be arbitrary. For simplicity, a uniform mesh of size $N \times N$, i.e., $\Delta x = \Delta y$, is employed.

3.1. Hollow circular waveguide

We first consider a hollow circular waveguide with a radius $R = 1$. The physical parameters are selected as $\epsilon = 1$ and $\lambda = 1$. This example has been previously studied in [4] and the analytical result is known to be $\beta_e = 0.95610217441041$ [4,23] for the first

dominate mode, i.e., the fundamental mode. This fundamental mode is an transverse electric (TE) mode, since it can be expressed in a form in which $E_z = 0$. Moreover, in the literature [23], this TE mode is commonly referred to as the TE_{11} mode, which has the smallest cutoff frequency for the circular waveguide.

In present study, we choose domain size $a = \pi/2$ and consider different mesh size N. The absolute errors in β_e of the ray-casting MIB method are depicted as a dashed line in Fig. 3. A linear fitting by means of the least squares (LS) is then conducted in the log–log scale [16] and the fitted convergence line is shown as a solid line in Fig. 3. Moreover, the fitted slope essentially represents the numerical convergence rate r of the MIB scheme. For this simple hollow waveguide, a over-performance rate $r = 6.03$ is numerically detected. This demonstrates the superior accuracy of the proposed MIB scheme. The components H^x and H^y of the fundamental mode are depicted in Fig. 4. It can be seen that in general both H^x and H^y are nonzero at the PEC boundary. The PEC boundary is treated as an immersed boundary in the present Cartesian grid method with a square computational domain. In the perfect conductor, the values of H^x and H^y are physically undefined, while in numerical experiments, they are simply taken as zeros.

3.2. Partially filled circular waveguide

We note that by using an isoparametric finite element method, up to the 6th order of accuracy has been achieved in [4] for solving the hollow circular waveguide. However, when applying that method to inhomogeneous waveguides, the convergence rate becomes essentially second order [4]. It is thus of great interest to investigate the performance of the proposed MIB method for solving inhomogeneous waveguides. To this end, we consider a partially filled circular waveguide with an interior circular interface and an exterior circular PEC boundary. The radius is chosen to be $R_1 = 1$ and $R_2 = 2$, respectively, for the interface and PEC boundary. A step-index profile is considered, i.e., $\epsilon = \epsilon_1$ for $\rho < R_1$ and $\epsilon = \epsilon_2$ for $R_1 < \rho < R_2$. Two sets of dielectric constants will be considered, one with low contrast (Case 1) and another with high contrast (Case 2). In both cases, the wavelength is fixed to be $\lambda = 2$ and the cladding region is assumed to be the air, i.e., $\epsilon_2 = 1$. For the core region, ϵ_1 is chosen to be $\epsilon_1 = 2.25$ and $\epsilon_1 = 12.25$, respectively, for the Cases 1 and 2. The analytical eigenvalues of the fundamental modes are available [23] to be $\beta_e = 1.358971746062259$ and 3.422561765974605, respectively, for Cases 1 and 2.

The complete MIB discretization is generated by using the previously developed MIB scheme [18,19] for treating the interface and the present ray-casting MIB scheme for dealing with the PEC boundary. By setting the domain dimension to be $a = 2 + \pi/3$, the numerical results of both cases are depicted in Fig. 5. Here, both the MIB errors in terms of $|\beta_e|$ (dashed lines) and the corresponding fitted convergence lines (solid lines) are shown. For Cases 1 and 2, the numerical order r is calculated to be 4.60 and 4.66, respectively. Since the MIB interface scheme has been shown to be of the fourth order of accuracy in [18,19], the present results verify the fourth order convergence of the proposed ray-casting MIB method. Furthermore, the present results also indicate the robustness of the MIB approach for dealing with high contrast index profiles.

The H^x and H^y components of the fundamental mode for the low contrast case are shown in Fig. 6. Here, both real and imaginary

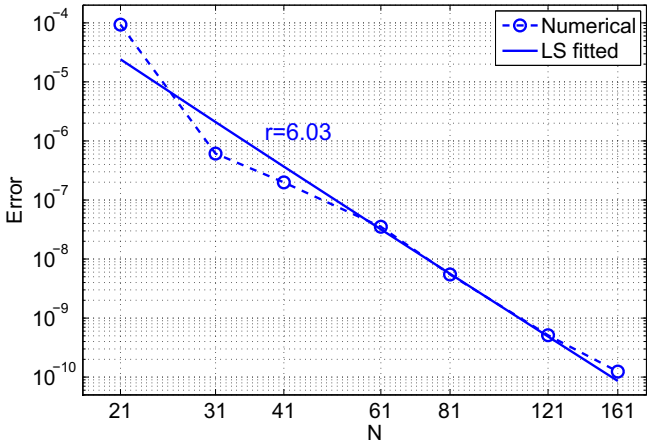

Fig. 3. Numerical convergence rate for the hollow circular waveguide.

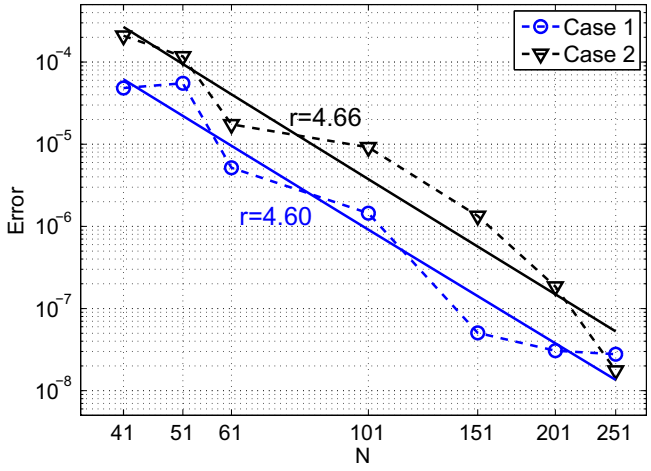

Fig. 5. Numerical convergence rates for the partially filled circular waveguide.

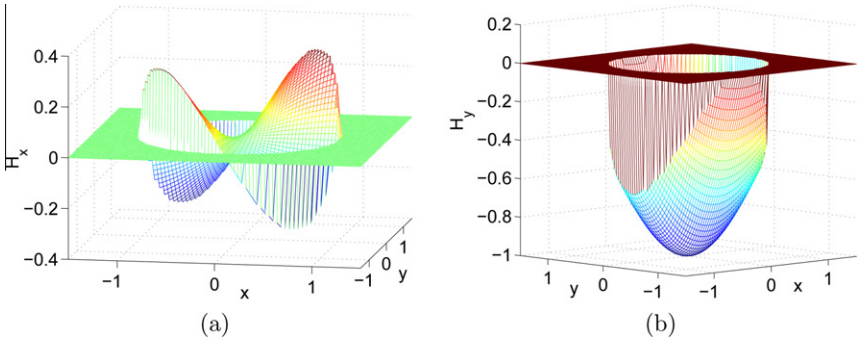

Fig. 4. The fundamental mode of the hollow circular waveguide. (a) H^x and (b) H^y.

parts of the field components are presented, because the numerical fundamental mode is complex in the present study. In fact, both eigenvalues β_e and eigenfunctions of two index profiles keep to be complex for the present partially filled circular waveguide, when different mesh size N and different tolerance in the iterative eigen-solver [24] are chosen. Even though the fundamental modes of a lossless waveguide should theoretically take real values, the MIB discretized matrix is not symmetric. Thus, numerically it might produce complex eigenvalues. Similar situation has been seen in other MIB studies [19]. Moreover, in consistent with our findings in [19], the imaginary part of the present eigenvalue, i.e., $Im(\beta_e)$, is usually very small. For example, when taking $N = 61$, $Im(\beta_e)$ is on the order of 10^{-7}–10^{-6}. Thus, its contribution to the magnitude $|\beta_e|$ is comparable to the double precision limit. In other words, such a contribution is negligible when computing $|\beta_e|$. Meanwhile, we note that $Im(\beta_e)$ is usually smaller than the corresponding MIB error, which is about 10^{-6}–10^{-5} for $N = 61$ (see Fig. 5). Therefore, it is believed that when using a larger and larger mesh size N, the MIB results will converge to the true real-valued physical mode.

Even though the MIB eigenfunctions are complex, some in-depth understanding of physics can still be revealed through their graphs. First, it can be observed from Fig. 6 that all eigenmodes are well confined within the PEC boundary. This can also be seen in the contour plots in Fig. 7. Physically, such a confinement is because of the exponential decay of eigenfunctions in the cladding region ($1 < \rho < 2$). Nevertheless, a closer investigation indicates that again H^x and H^y are nonzero at the PEC boundary, but attain small values on the order of 10^{-3}. Second, it is known that for the partially filled circular waveguide, only a rotationally symmetric field can be either transverse electric (TE) or transverse magnetic (TM), while the fundamental mode is neither TE nor TM [23]. The contour plots of H^x and H^y in Fig. 7 clearly show that our numerical fundamental fields are not rotationally symmetric fields. Thus, they are neither TE nor TM. However, under the limit of $\epsilon_2 \to \epsilon_1$, this fundamental mode will reduce to the TE_{11} mode of the empty waveguide.

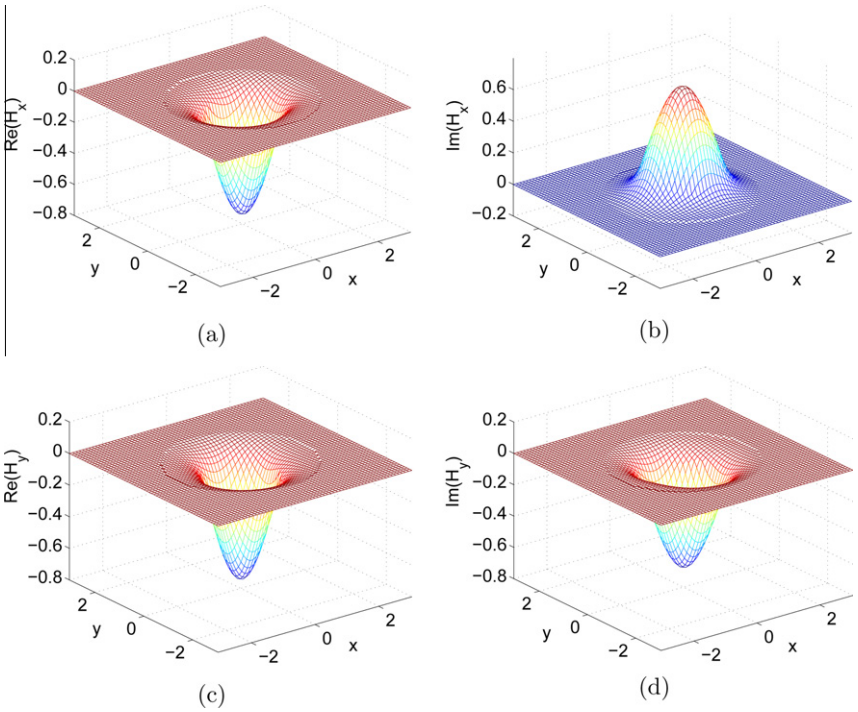

Fig. 6. The fundamental mode of the partially filled waveguide. (a) The real part of H^x; (b) the imaginary part of H^x; (c) the real part of H^y and (d) the imaginary part of H^y.

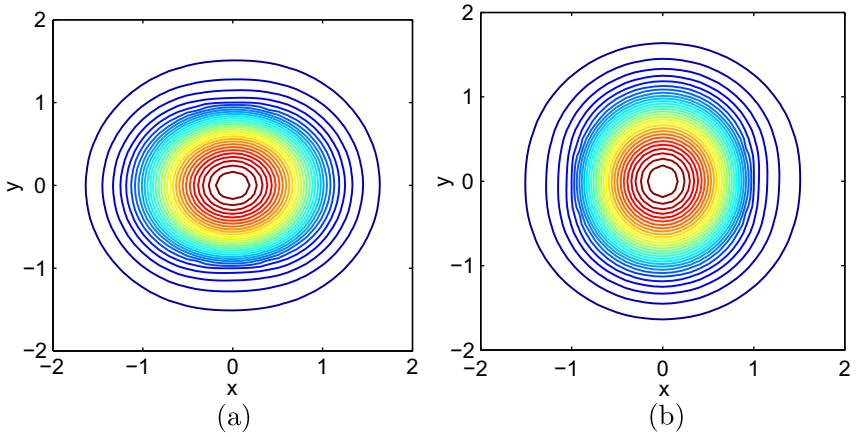

Fig. 7. Contour plots of the fundamental mode of the partially filled waveguide. (a) $|H^x|$ and (b) $|H^y|$.

3.3. Coaxial waveguide

We finally consider a coaxial waveguide with perfect conductors being located both inside a radius $R_1 = 0.75$ and outside a radius $R_2 = 2$. The physical parameters are chosen as $\epsilon = 2.25$ and $\lambda = 1$. Two dominate modes are considered in the present study. The fundamental mode of the coaxial waveguide is known to be a transverse electromagnetic (TEM) mode [23], which exists when both E_z and H_z equal to zero. The corresponding eigenvalue is fixed to be $\beta_e = 1.5$, no matter what values of R_1, R_2, ϵ and λ are employed. Thus, in some engineering context, such a mode might be referred to as a boundary mode, because it is induced by the two conductor boundary structure, not by the interior dielectric profile. Computationally, the study of the fundamental mode is sufficient to test the proposed algorithm under different model parameters. We thus consider the second dominate mode, i.e., the TE_{11} mode with an analytical eigenvalue $\beta_e = 1.495301277452637$ [23]. The TE_{11} mode depends on the structure and dielectric profile.

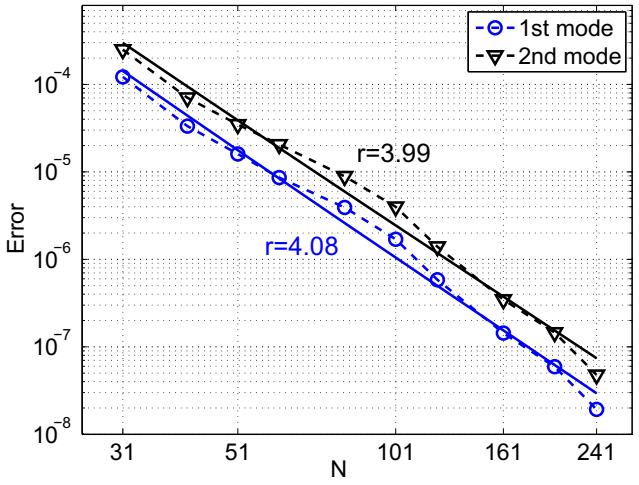

Fig. 8. Numerical convergence rates for the coaxial waveguide. First mode: the TEM mode. Second mode: the TE_{11} mode.

Numerically, to account for the two conductor structure, two reversal ray-casting processes will be conducted, because the outward normal directions for the both PEC boundaries are opposite. A fully automatic MIB implementation is coded so that the same subroutine can handle both situations. The MIB error and corresponding convergence line for both TEM and TE_{11} modes are depicted in Fig. 8. Clearly, the MIB method attains exactly the fourth order of convergence rate in both cases. The H^x and H^y components of two dominate modes are plotted in Fig. 9. In all charts, the eigenfunctions are vanishing in the interior and exterior perfect conductors. Moreover, it can be seen from Fig. 9 that the eigenfunctions of the TE_{11} mode undergo a sharp increment along the ρ direction near the inner PEC boundary $R_1 = 0.75$. Mathematically, it is known that the analytical Bessel solution of this problem is singular at the origin [23], if it is extended to the whole domain. Such a rapid variation is difficult to be resolved by using a low order finite difference method, while the present higher order approach demonstrates excellent results in simulating such a problem.

At last, we study the computational efficiency of the MIB method. Computationally, the CPU time spend for the MIB fictitious domain generation is usually much less than that consumed by solving the eigen-system via a standard iterative solver [24]. Although the bandwidth of the MIB method is as large as 60 for each irregular node, such a bandwidth is fixed for different mesh size N. On the other hand, the total number of irregular nodes increases with respect to the mesh size N linearly, because the number of total irregular points is one-dimension lower than the number of total grid points. Thus, the computational overhead of the MIB treatments essentially scales as $O(N)$. We demonstrate this by testing the CPU times of the MIB preprocessing in solving the coaxial waveguide, see Table 1. The linear trend is clearly seen for the MIB CPU times and the MIB overhead consumes a negligible

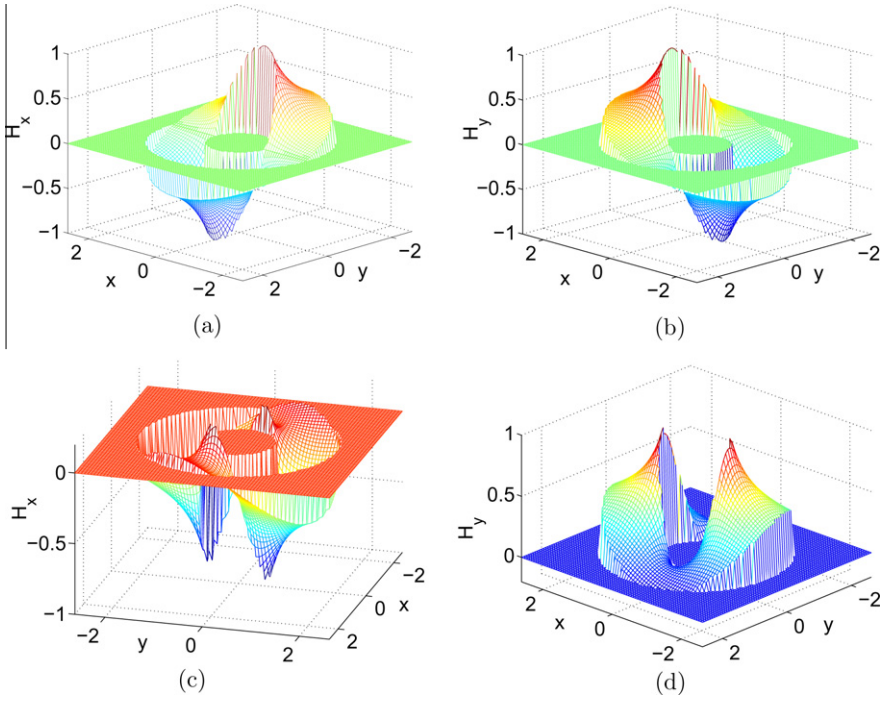

Fig. 9. The dominate modes of the coaxial waveguide. (a) H^x component of the TEM mode; (b) H^y component of the TEM mode; (c) H^x component of the TE_{11} mode and (d) H^y component of the TE_{11} mode.

Table 1
Numerically detected CPU times for the coaxial waveguide (measured in second).

N	31	61	121	241
MIB	2.00×10^{-3}	3.99×10^{-3}	7.99×10^{-3}	1.59×10^{-2}
Total	3.48	3.23×10^{1}	6.87×10^{3}	2.14×10^{5}

amount of time comparing with the total CPU time. This is in consistent with the findings in our previous studies [18].

4. Conclusion

In conclusion, we have introduced a novel ray-casting MIB method for solving curved PEC boundaries. The previously developed MIB scheme for solving dielectric interface problems [18,19] is not applicable to treat the PEC wall, because the PEC boundary conditions have a physical nature quite different from that of the jump conditions at the dielectric interface. In particular, all six electric and magnetic field components are prescribed in the jump conditions, whereas only three of them are known at the PEC wall. A novel ray-casting process is proposed in this work to enforce the PEC boundary conditions only along the normal directions. Such a process is effectively coupled with the overall fictitious domain generation of the MIB approach. The fourth order convergence of the ray-casting MIB method is numerically confirmed for both homogeneous and inhomogeneous waveguides. The CPU time for the MIB preprocessing has been shown to be negligible in numerical computations. The testing of the proposed MIB method for more complex geometry is currently under investigation. We finally note that as in [18,19] the curved PEC boundaries considered in this work are C^1 continuous. This is because very likely the higher order methods will be degraded to the second order if the geometry boundary is only C^0 continuous, due to the corner singularity problems [14–16].

Acknowledgments

This work was supported in part by NSF Grants DMS-0616704 and DMS-0731503, and by a UA Research Grants Committee Award. The author would like to thank anonymous referees for their many insightful comments that improved the paper.

References

[1] G.R. Hadley, Numerical simulation of waveguides of arbitrary cross-section, Int. J. Electron. Commun. 58 (2004) 86–92.
[2] P.-J. Chiang, C.-L. Wu, C.-H. Teng, C.-S. Yang, H.-C. Chang, Full-vectorial optical waveguide mode solvers using multidomain pseudospectral frequency-domain (PSFD) formulations, IEEE J. Quantum Electron. 44 (2008) 56–66.
[3] M. Koshiba, Y. Tsuji, Curvilinear hybrid edge/nodal elements with triangular shape for guide-wave problems, J. Lightwave Technol. 18 (2000) 737–743.
[4] K. Dossou, M. Fontaine, A high order isoparametric finite element method for the computation of waveguide modes, Comput. Method Appl. Mech. Engrg. 194 (2005) 837–858.
[5] N. Marais, D.B. Davidson, Numerical evaluation of hierarchical vector finite elements on curvilinear domains in 2D, IEEE Trans. Antenn. Propag. 54 (2006) 734–738.
[6] B.M. Notaros, Higher order frequency-domain computational electromagnetics, IEEE Trans. Antenn. Propag. 56 (2008) 2251–2276.
[7] S. Dey, R. Mittra, A locally conformal finite-difference time-domain (FDTD) algorithm for modeling three-dimensional perfectly conducting objects, IEEE Microwave Guided Wave Lett. 7 (1997) 273–275.
[8] W. Yu, R. Mittra, A conformal FDTD algorithm for modeling perfectly conducting objects with curved-shaped surfaces and edges, Microwave Opt. Tech. Lett. 27 (2000) 136–138.
[9] T. Xiao, Q.H. Liu, Enlarged cells for the conformal FDTD method to avoid the time step reduction, IEEE Microwave Compon. Lett. 14 (2004) 551–553.
[10] S. Benkler, N. Chavannes, N. Kuster, A new 3D conformal PEC FDTD scheme with user-defined geometric precision and derived stability criterion, IEEE Trans. Antenn. Propag. 54 (2006) 1843–1849.
[11] M.T. Bettencourt, Flux limiting embedded boundary technique for electromagnetic FDTD, J. Comput. Phys. 227 (2008) 3134–3158.
[12] A.-K. Tornberg, B. Engquist, Consistent boundary conditions for the Yee scheme, J. Comput. Phys. 227 (2008) 6922–6943.
[13] S. Zhao, G.W. Wei, High-order FDTD methods via derivative matching for Maxwell's equations with material interfaces, J. Comput. Phys. 200 (2004) 60–103.
[14] G.R. Hadley, High-accuracy finite-difference equations for dielectric waveguide analysis II: Dielectric corners, J. Lightwave Technol. 20 (2002) 1219–1231.
[15] N. Thomas, P. Sewell, T.M. Benson, A new full-vectorial higher order finite-difference scheme for the modal analysis of rectangular dielectric waveguides, J. Lightwave Technol. 25 (2007) 2563–2570.
[16] S. Zhao, Full-vectorial matched interface and boundary (MIB) method for the modal analysis of dielectric waveguides, J. Lightwave Technol. 26 (2008) 2251–2259.
[17] Y.C. Chiang, Y.P. Chiou, H.C. Chang, Improved full-vectorial finite-difference mode solver for optical waveguides with step-index profiles, J. Lightwave Technol. 20 (2002) 1609–1618.
[18] S. Zhao, High order vectorial analysis of waveguides with curved dielectric interfaces, IEEE Microwave Compon. Lett. 19 (2009) 266–268.
[19] S. Zhao, High order matched interface and boundary methods for the Helmholtz equation in media with arbitrarily curved interfaces, J. Comput. Phys. 229 (2010) 3155–3170.
[20] S. Zhao, On the spurious solutions in the high-order finite difference methods, Comput. Method Appl. Mech. Engrg 196 (2007) 5031–5046.
[21] S. Zhao, G.W. Wei, Matched interface and boundary (MIB) method for the implementation of boundary conditions in high-order central finite differences, Int. J. Numer. Method Engrg. 77 (2009) 1690–1730.
[22] Y.C. Zhou, S. Zhao, M. Feig, G.W. Wei, High order matched interface and boundary (MIB) schemes for elliptic equations with discontinuous coefficients and singular sources, J. Comput. Phys. 213 (2006) 1–30.
[23] R.F. Harrington, Time-Harmonic Electromagnetic Fields, Wiley–IEEE Press, 2001.
[24] Z. Bai, G.W. Stewart, SRRIT: a Fortran subroutine to calculate the dominant invariant subspace of a nonsymmetric matrix, ACM Trans. Math. Software 23 (1997) 494–513.